frontiers | Frontiers in Energy Research

TYPE Original Research
PUBLISHED 20 November 2024
DOI 10.3389/fenrg.2024.1507604

OPEN ACCESS

EDITED BY
Haifeng Qiu,
Nanyang Technological University, Singapore

REVIEWED BY
Yu Huang,
Nanjing University of Posts and Telecommunications, China
Lingling Wang,
Shanghai Jiao Tong University, China
Yucui Wang,
North China Electric Power University (Baoding), China

*CORRESPONDENCE
Wendi Wang,
sy584278874@163.com

RECEIVED 08 October 2024
ACCEPTED 06 November 2024
PUBLISHED 20 November 2024

CITATION
Wang W, Huang H, Zhang X, Tan J and Sun S (2024) Flexible low carbon optimal dispatch of distribution networks considering the demand response of heat storage industrial loads. *Front. Energy Res.* 12:1507604. doi: 10.3389/fenrg.2024.1507604

Flexible low carbon optimal dispatch of distribution networks considering the demand response of heat storage industrial loads

Wendi Wang[1]*, Hao Huang[1], Xinsheng Zhang[2], Jie Tan[3] and Shaobin Sun[1]

[1]Nanjing Suyi Industrial Co., Ltd., Technology Information Network Branch, Nanjing, China, [2]Nanjing Suyi Industrial Co., Ltd., Nanjing, China, [3]Nanjing Huaqun Energy Group Co., Ltd., Nanjing, China

To cope with the uncertainty brought by the large-scale integration of renewable energy under the goal of carbon neutrality, it is necessary to tap and utilize flexible and adjustable resources from both the source and the load side at the same time. Hence, a flexible low-carbon optimal scheduling method for distribution networks is proposed in this paper, which takes into account the participation of heat storage industrial loads in demand response. Firstly, the model of the gas turbine equipped with a flexible carbon capture device is established, and the non-convex constraint introduced by the adjustable flue gas diversion ratio is convexified. Then the model of the fused magnesium load, a representative of heat storage industrial loads, is established for its participation in demand response. The segment linearization and convexification methods are performed on the conditional productivity constraints of the fused magnesium load. On this basis, a mixed-integer linear programming model for flexible and low-carbon optimal dispatch of the distribution network is developed by using the stochastic optimization theory and solved by commercial solvers. The proposed method is verified to be able to ensure the economic operation of the distribution network while reducing carbon emissions and promoting renewable energy consumption.

KEYWORDS

heat storage industrial loads, demand response, carbon capture devices, flexible low-carbon optimal dispatch, renewable energy

1 Introduction

As energy shortages and global warming issues have become increasingly severe, the major countries of the world have signed the Paris Agreement. Since the power industry is a major source of carbon emissions, these countries are vigorously promoting the deployment of renewable energy sources (RES) to relieve the pressure of decarbonization and achieve the anticipated emission reduction targets (Xu et al., 2023; Xu and Yi, 2023). However, the uncertainty, volatility, and anti-peak characteristics of the RES output pose a huge challenge to the stable operation of the system (Cheng et al., 2023; Tan et al., 2019). Since the distribution network is integrated with various types of distributed RES, how to ensure the

continuity and reliability of power supply is a particularly evident challenge (Zhang et al., 2024; Zhang et al., 2023; Huang et al., 2020).

To address the challenges of integrating RES, gas turbines and demand response are becoming attractive measures (Zhang and Zhu, 2024; Condessa et al., 2023; de Chalendar et al., 2023). Gas turbines are an ideal choice as backup power sources for RES due to their high efficiency and relatively low carbon emissions. However, to achieve the emission reduction and the carbon neutrality targets, even gas turbines need further decarbonization. Gas turbines installed with flexible carbon capture technology (FCCGT) have high commercial maturity and do not require large-scale retrofits to the existing gas turbine, which is a promising technology to reduce carbon emissions (Fan et al., 2023). It is proposed in (Wilkes et al., 2021) that the quick-response capability of gas turbines is indispensable for providing system flexibility. When combined with post-combustion carbon capture technology, gas turbines offer critical support for the transition to a future low-carbon society. Integrating flexible combined-cycle gas turbines with carbon capture and storage technology is investigated and analyzed in (Chyong et al., 2023) for constructing low-carbon power systems. A laddered carbon trading-based operation model is proposed in (Gao et al., 2024) for an integrated electricity-gas system considering the complex combustion properties of hydrogen mixed gas turbine. In (Wang et al., 2022), the liquid storage carbon capture and power to gas technologies are applied to construct a coordinated heat and power operation model, which takes into account the carbon trading cost. Besides, due to the large thermal inertia of the heat storage industrial loads (HSIL), their operating power can be rapidly adjusted upward or downward with little impact on the production process, which play an important role in the demand-side management of the distribution network. Through demand response (DR) technology, HSIL can be flexibly dispatched within a certain range, which improves the matching degree of load demand and RES output and enhance the stability of the distribution system (Boldrini et al., 2024; Shao et al., 2021). Hence, exploiting the DR potential of HSIL helps balance the power supply and demand to enable the increase of RES integration, which indirectly contributes to carbon emission reduction (Wang J. et al., 2023). As one of the representative HSIL, magnesium load using an electric arc furnace (MLEAF) has a simple production process, but can provide significant regulation capability due to its thermal inertia. Therefore, modelling the DR participation of MLEAF with a low complexity has become a research focus in recent years. A novel adaptive Proportional-Integral-Derivative controller has been developed to regulate the melting current of MLEAF within desired parameters, resulting in significant energy savings (Wang W. et al., 2023). Based on a comprehensive analysis of the characteristics of electrical arc furnace, a refined model of MLEAF is developed in (Wang et al., 2024). Besides, a low-carbon dispatch method is proposed in (Zhao et al., 2024) to consider the demand regulation of MLEAF and the fluctuation of wind power generation, which achieves stable and reliable operation of the power system through the integration of thermal power plants and the introduction of battery energy storage systems.

However, there are still many challenges about how to effectively integrate FCCGT and the DR capacity of HSIL to relieve the distribution network dispatch pressure:

1) The uncertainty and anti-peak characteristics of RES output place higher requirements on the response speed and flexibility of the distribution network. If the RES output is low during load peaks, it will inevitably lead to an increase in FCCGT and carbon emissions, requiring the capture and processing of more CO_2. In this case, the power consumption of the carbon capture (CC) device of FCCGT increases accordingly, bringing extra load to the load peaks. This phenomenon is called "peak-on-peak," which severely damages the power balance of the distribution network.
2) The large-scale utilization of flexible resources from both the supply and demand sides increases the complexity of the distribution network optimal dispatch model. Unreasonable modeling methods and solving algorithms not only fail to improve the economic efficiency of the dispatch plan but may even threaten the safety of distribution network operation and load power supply (Qi et al., 2023; Gabrielli et al., 2022). For example, the HSIL equipment's working temperature has impacts on the production output and quality, so the changes in temperature need strict limits. If these impacts and limits are ignored in the DR model, the actual response willingness of HSIL may be much lower than expected, which brings greater pressure in turn to the distribution network operation (Wang et al., 2024; Yue et al., 2024).

To solve the problems above, a flexible low-carbon optimal dispatch model is proposed for the distribution network in this paper, which contains the models of FCCGT and a representative HSIL, i.e., MLEAF. The contributions of this model are listed below:

1) The model of FCCGT with storage tanks is constructed, where the non-linear constraints related to the adjustable flue gas diversion ratio is convexified by the McCormick envelope method.
2) The model for the DR participation of MLEAF is proposed, where 0-1 auxiliary variables are introduced to construct the piece-wise function-based production output constraints and the resulting bilinear terms are convexified.
3) Based on the models of FCCGT and MLEAF, a mixed-integer linear stochastic optimization model is established with typical forecast error scenarios of RES and load to realize the low-carbon dispatch of the distribution network, which can be solved by commercial solvers such as CPLEX.

The rest of the paper is organized as follows. In Section 2, the operation mechanism is analyzed and the linearized model is constructed for FCCGT. In Section 3, the DR model of MLEAF is established where the production output constraints are convexified. Then the flexible low-carbon optimal dispatch model of the distribution network is detailed with its objective function and constraints in Section 4. Numerical tests are performed on a modified IEEE 33-bus system and the results are discussed in Section 5. The conclusions are summarized in Section 6.

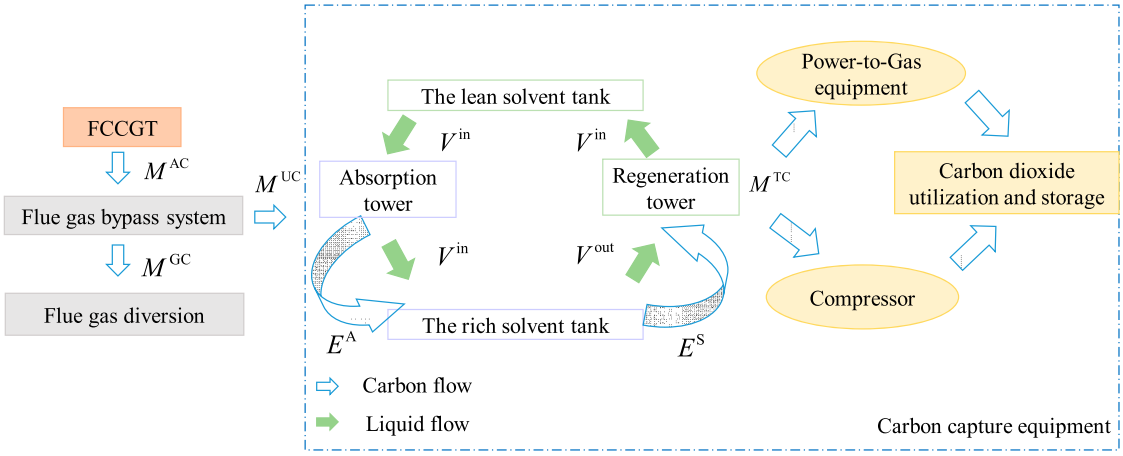

FIGURE 1
Integrated flexible operation process of FCCGT.

2 FCCGT operation mechanism and mathematical model

2.1 FCCGT structure and operation mode

Based on the combustion process, CC technologies can be classified into oxy-fuel combustion, pre-combustion capture, and post-combustion capture. Based on the operating modes, they can be divided into slipstream mode, storage mode, and integrated flexible operation mode.

Considering the commercial and technological maturity, the post-combustion capture technology with integrated flexible operation mode is adopted by FCCGT, which is realized by installing a flue gas bypass system and a solvent storage tank on the gas turbine (Song et al., 2024). The operation process of FCCGT is shown in Figure 1.

FCCGT controls the flue gas bypass system to feed a certain proportion of the flue gas generated by the gas turbine into the absorption tower. In this tower, the flue gas reacts with an ethanolamine (MEA) solution to obtain a CO_2-rich solution, which is stored in the rich solution storage tank. The rich solution pump is then adjusted to control the rich solution fed to the regeneration tower, where the rich solution is heated with extracted steam to cause counter-reaction to separate CO_2 from the MEA. The separated CO_2 is partially used as feedstock of a power-to-gas facility to produce methane for the natural gas network, while the remaining CO_2 is compressed for storage. The regenerated lean MEA solution is pumped back into the lean solution storage tank and recirculated to the absorption tower for reuse. This integrated flexible operation allows FCCGT to efficiently capture and utilize the CO_2 generated by the gas turbine.

Compared to gas turbines equipped with traditional CC device, the unique features of FCCGT are:

1. Flexible and controllable flue gas diversion ratio: By adjusting the flue gas bypass system, the proportion of flue gas entering the CC device can be controlled, allowing a balance between operating costs and carbon emissions.
2. Flexible carbon capture based on solution storage tanks: The CC amount is decoupled with the CC power consumption, which leads to a wider range of net power output of FCCGT. Such CO_2 processing flexibility serves as a supplementary resource to promote the consumption of RES power and contribute to the power balance of the distribution network.

Due to these distinctive features, a targeted model needs to be established for FCCGT.

2.2 The mathematical model of FCCGT

According to Figure 1, the model reflecting the power output and real-time CC amount of FCCGT is expressed as follows:

$$\begin{cases} P_t^{\mathrm{FCC}} = P_{\mathrm{e},t}^{\mathrm{FCC}} + \chi M_t^{\mathrm{TC}} + P_t^{\mathrm{Y}} \\ M_t^{\mathrm{TC}} = M_t^{\mathrm{UC}} + E_t^{\mathrm{S}} - E_t^{\mathrm{A}} \\ M_t^{\mathrm{UC}} = \theta_{\max}^{\mathrm{CC}} \gamma^{\mathrm{FCC}} \delta_t P_t^{\mathrm{FCC}} \\ M_t^{\mathrm{AC}} = \gamma^{\mathrm{FCC}} P_t^{\mathrm{FCC}} \\ M_t^{\mathrm{GC}} = M_t^{\mathrm{AC}} - M_t^{\mathrm{UC}} \\ \delta_{\min} \le \delta_t \le \delta_{\max}, P_{\min}^{\mathrm{FCC}} \le P_t^{\mathrm{FCC}} \le P_{\max}^{\mathrm{FCC}} \\ 0 \le M_t^{\mathrm{TC}} \le \eta \theta_{\max}^{\mathrm{CC}} \gamma^{\mathrm{FCC}} P_{\max}^{\mathrm{FCC}} \end{cases} \tag{1}$$

where t is the index of time. P_t^{FCC} is the total power output of FCCGT. $P_{\mathrm{e},t}^{\mathrm{FCC}}$ is the net power delivered to the distribution network by FCCGT. P_t^{Y} is the CC power consumption of the CC device. χ is the consumed power for capturing unit mass of CO_2 (MWh/t). M_t^{TC} is the total mass of the captured CO_2, M_t^{UC} is the mass of CO_2 entering the CC device after flue gas diversion (t). E_t^{S} is the mass of CO_2 supplied from the rich solution storage tank (t). E_t^{A} is the mass of CO_2 absorbed by the rich solution storage tank (t). δ_t is the flue gas diversion ratio. $\theta_{\max}^{\mathrm{CC}}$ is the maximum CC level. M_t^{AC} is the total mass of CO_2 produced by FCCGT (t). γ^{FCC} is the CO_2 emission intensity of FCCGT (t/MWh). M_t^{GC} is the mass of CO_2 emitted into the atmosphere from FCCGT after flue gas diversion (t). $P_{\max}^{\mathrm{FCC}}$ and $P_{\min}^{\mathrm{FCC}}$ are the upper and lower power limits of FCCGT.

According to (Equation 1), by controlling the inflow and outflow of the rich solution storage tank, the amount of CO_2 flowing into the absorption tower M_t^{UC} can be different from that processed by regeneration tower M_t^{AC} at the same time, which realizes the decoupling of CC amount and power consumption mentioned in the Introduction.

Since the CO_2 is stored in the solution in the state of MEA compound, the variables related to the mass of CO_2 in (Equation 1) should be converted the volume of MEA solution, which is then used to model the volumetric constraints of the solution storage tanks. The conversion between CO_2 mass and MEA volume is shown as:

$$\begin{cases} V_t^{in} = \dfrac{E_t^A M^{MEA}}{\psi S_t^{MEA} \rho_t^{MEA} M^{CO_2}} \\ V_t^{out} = \dfrac{E_t^S M^{MEA}}{\psi S_t^{MEA} \rho_t^{MEA} M^{CO_2}} \end{cases} \tag{2}$$

where V_t^{in} and V_t^{out} are the MEA volume flowing into/out of the rich solution storage tank (m^3). M^{MEA} and M^{CO_2} are the molar masses of MEA and CO_2 (g/mol). ψ is the mass of CO_2 that can be absorbed by 1 mol of MEA (mol/mol). S_t^{MEA} is the solution concentration. ρ_t^{MEA} is the solution density (t/m^3).

Then the volumetric constraints of the solution storage tanks can be modeled as follows:

$$\begin{cases} V_t^F = V_{t-1}^F - V_t^{out} + V_t^{in} \\ V_t^W = V_{t-1}^W + V_t^{out} - V_t^{in} \\ V_0^F = V_T^F \\ 0 \le V_t^F \le V^L, 0 \le V_t^W \le V^L \end{cases} \tag{3}$$

where V_t^{FL} and V_t^{WL} are the MEA volumes in the rich and lean solution storage tanks at time t, respectively. V_{t-1}^{FL} and V_{t-1}^{FL} are the MEA volumes in the rich and lean solution storage tanks at time t-1, respectively. V_0^{FL} and V_T^{FL} are the MEA volumes in the rich solution storage tank at time 0 and T, respectively. T is the total time slots in a dispatching cycle. V^L is the volume of the solution storage tanks (m^3).

Besides, the solution storage tanks should not flow in and out MEA simultaneously, and the inflow and outflow have upper limits, which are expressed as follows.

$$\begin{cases} 0 \le E_t^S \le \eta \theta_{max}^{CC} \gamma^{FCC} P_{max}^{FCC} U_t^W \\ 0 \le E_t^A \le \eta \theta_{max}^{CC} \gamma^{FCC} P_{max}^{FCC} U_t^F \\ 0 \le E_t^A \le M_t^{TC} \\ U_t^W + U_t^F = 1 \end{cases} \tag{4}$$

where η is the maximum operational efficiency of the regenerator tower and the compressor. U_t^W and U_t^F are the 0-1 indicator variables reflecting the MEA volume changes in the lean and rich solution storage tanks, respectively.

2.3 The convexification of the FCCGT model

The bilinear term $\delta_t P_t^{FCC}$ in (Equation 1) leads to a non-convex FCCGT model. To convexify this bilinear term, McCormick envelopes are used and shown as below (Deng et al., 2021).

$$\omega_t = \delta_t P_t^{FCC} \tag{5}$$

$$\begin{cases} \omega_t \ge \delta_{min} P_t^{FCC} + \delta_t P_{t,min}^{FCC} - \delta_{min} P_{t,min}^{FCC} \\ \omega_t \ge \delta_{max} P_t^{FCC} + \delta_t P_{t,max}^{FCC} - \delta_{max} P_{t,max}^{FCC} \\ \omega_t \le \delta_{max} P_t^{FCC} + \delta_t P_{t,min}^{FCC} - \delta_{max} P_{t,min}^{FCC} \\ \omega_t \le \delta_t P_{t,max}^{FCC} + \delta_{min} P_t^{FCC} - \delta_{min} P_{t,max}^{FCC} \end{cases} \tag{6}$$

where ω_t is an auxiliary variable used to replace $\delta_t P_t^{FCC}$ in (Equation 1). Therefore, By combining the replaced (Equations 1, 6), the proposed FCCGT model is convexified.

3 The demand response model for MLEAF

MLEAF utilizes the heat generated by the alternating current arc to heat the dolomite ore to a molten state to obtain magnesium oxide crystals, so MLEAF is a representative high-energy-consuming HSIL. The MLEAF can control its load power by adjusting the electrodes with an electrode controller, which regulates the current within the furnace. Even if regulated with a small percentage of the rated power, MLEAF can effectively supplement the regulation capacity required by the distribution network, serving as a flexible DR resource. The specific model is described as follows.

3.1 The MLEAF model

Based on the production principles and operating modes of the MLEAF, its DR model for day-ahead optimal dispatch is constructed, which consists of the following constraints.

(1) Constraints of MLEAF regulatable capacity

$$\begin{cases} P_{m,t} = P_m^{base} + P_{m,t}^u - P_{m,t}^d \\ su_{m,t} + sd_{m,t} \le 1 \\ 0 \le P_{m,t}^u \le su_{m,t} P_{max}^u \\ 0 \le P_{m,t}^d \le sd_{m,t} P_{max}^d \end{cases} \tag{7}$$

where $P_{m,t}$ is the operating power of the MLEAF after regulation. P_m^{base} is the rated power of the MLEAF. $P_{m,t}^u$ and $P_{m,t}^d$ are the power increment and decrement of the MLEAF. $su_{m,t}$ and $sd_{m,t}$ are the 0-1 variables indicating the upward and downward regulation states of MLEAF, respectively. P_{max}^u and P_{max}^d are the maximum power increment and decrement of the MLEAF while ensuring safe operation.

(2) The constraints of regulation times of MLEAF

During a complete production cycle, the regulation times for each MLEAF should not exceed the predetermined upper limits to avoid adverse impact on the product purity. The relevant constraints are shown as follows:

$$\begin{cases} y_{m,t} - z_{m,t} = su_{m,t} - su_{m,t-1} \\ y_{m,t} + z_{m,t} \le 1 \\ \sum y_{m,t} + \sum z_{m,t} \le M \end{cases} \tag{8}$$

where $y_{m,t}$ and $z_{m,t}$ are the 0-1 variables indicating that MLEAF changes to the upward and downward regulation states, respectively. M is the maximum regulation times of the MLEAF.

(3) The constraints of the MLEAF production output

To ensure that the MLEAF production output still meets requirements after participating in the DR project, the following constraints are constructed:

$$\sum_{t=1}^{T} \lambda(P_{m,t}) \cdot P_{m,t} \geq O_m \tag{9}$$

where O_m is the target of MLEAF production output. $\lambda(P_{m,t})$ is the piecewise linear function of the MLEAF yield to its power, which is shown as

$$\lambda(P_{m,t}) = \begin{cases} \lambda_1, P_m^{\text{base}} - P_{\max}^{\text{d}} \leq P_{m,t} \leq P_m^{\text{r,d}} \\ \lambda_2, P_m^{\text{r,d}} \leq P_{m,t} \leq P_m^{\text{r,u}} \\ \lambda_3, P_m^{\text{r,u}} \leq P_{m,t} \leq P_m^{\text{base}} + P_{\max}^{\text{u}} \end{cases} \tag{10}$$

where λ_1、λ_2 and λ_3 are the MLEAF yield under the power decrease state, nominal state, and power increase state. $P_m^{\text{r,d}}$ and $P_m^{\text{r,u}}$ are the lower and upper limits of the rated state of MLEAF.

3.2 Linearization of MLEAF production output constraints

The MLEAF production output constraints given by Equations 9, 10 are conditional constraints, which cannot be solved by common commercial solvers directly. To address this problem, auxiliary variables are first used to perform piecewise linearization of (Equation 10):

$$\begin{cases} s_{m,t}^{\text{d}} + s_{m,t}^{\text{r}} + s_{m,t}^{\text{u}} = 1 \\ \lambda_{m,t} = \lambda_1 s_{m,t}^{\text{d}} + \lambda_2 s_{m,t}^{\text{r}} + \lambda_3 s_{m,t}^{\text{u}} \\ P_{m,t} \leq P_m^{\text{r,d}} s_{m,t}^{\text{d}} + P_m^{\text{r,u}} s_{m,t}^{\text{r}} + \left(P_m^{\text{base}} + P_{\max}^{\text{u}}\right) s_{m,t}^{\text{u}} \\ P_{m,t} \geq \left(P_m^{\text{base}} - P_{\max}^{\text{d}}\right) s_{m,t}^{\text{d}} + P_m^{\text{r,d}} s_{m,t}^{\text{r}} + P_m^{\text{r,u}} s_{m,t}^{\text{u}} \end{cases} \tag{11}$$

where $\lambda_{m,t}$ is the output yield of the m-th MLEAF at time t. $s_{m,t}^{\text{d}}$, $s_{m,t}^{\text{r}}$ and $s_{m,t}^{\text{u}}$ are 0–1 variables to indicate the three intervals of $P_{m,t}$ divided in (Equations 10).

Based on (Equations 9, 11) can be rewritten as:

$$\sum_{t} \lambda_{m,t} P_{m,t} \geq O_m \tag{12}$$

Similarly with (Equation 1), the bilinear term in (Equation 12) can also be convexified using McCormick envelopes:

$$\sum_{t} o_{m,t} \geq O_m \tag{13}$$

where $o_{m,t}$ is an auxiliary variable used to replace the bilinear term $\lambda_{m,t} P_{m,t}$ in (Equation 12).

Although $\lambda_{m,t}$ is discrete, it still has minimum and maximum values, which are λ_1 and λ_3, respectively. The minimum and maximum values $P_{m,t}$ of are $P_m^{\text{base}} - P_{\max}^{\text{d}}$ and $P_m^{\text{base}} - P_{\max}^{\text{d}}$, respectively. Using the maximum and minimum values of $\lambda_{m,t}$ and $P_{m,t}$, the linearized limits of $o_{m,t}$ is constructed as:

$$\begin{cases} o_{m,t} \geq \lambda_1 P_{m,t} + \lambda_{m,t}\left(P_m^{\text{base}} - P_{\max}^{\text{d}}\right) - \lambda_1\left(P_m^{\text{base}} - P_{\max}^{\text{d}}\right) \\ o_{m,t} \geq \lambda_3 P_{m,t} + \lambda_{m,t}\left(P_m^{\text{base}} + P_{\max}^{\text{u}}\right) - \lambda_3\left(P_m^{\text{base}} + P_{\max}^{\text{u}}\right) \\ o_{m,t} \leq \lambda_3 P_{m,t} + \lambda_{m,t}\left(P_m^{\text{base}} - P_{\max}^{\text{d}}\right) - \lambda_3\left(P_m^{\text{base}} - P_{\max}^{\text{d}}\right) \\ o_{m,t} \leq \lambda_{m,t}\left(P_m^{\text{base}} + P_{\max}^{\text{u}}\right) + \lambda_1 P_{m,t} - \lambda_1\left(P_m^{\text{base}} + P_{\max}^{\text{u}}\right) \end{cases} \tag{14}$$

Finally, the MLEAF production output constraints are composed of (Equations 11, 13, 14).

4 Flexible low-carbon optimal dispatch model of the distribution network

In the day-ahead optimal dispatch, the power curves of RES output and load is firstly forecasted. Then the historical forecast error data are used to construct forecast error scenarios. By combining the forecasted power curves with the forecast error scenarios, the day-ahead stochastic scenarios of RES output and load are obtained with their corresponding probabilities. On the basis of the scenarios, a flexible low-carbon stochastic optimal dispatch model is established for the distribution network by taking into account the CC amount and power consumption decoupling of FCCGT and the DR potential of MLEAF. The objective function and constraints of this dispatch model are detailed as below.

4.1 Typical scenario generation method

The scenario generation method in (Zhang et al., 2021) is adopted here, whose procedures are given below.

Step 1: Organize the historical forecast error data of RES and load power as a matrix.

Step 2: Compute the eigenvectors of the forecast error matrix. Based on the eigenvectors, the minimum volume enclosing ellipsoid of the historical error data points are determined.

Step 3: The circumscribed polyhedron of the ellipsoid is obtained by an expansion method. Then the coordinates of the vertices of the circumscribed polyhedron are the derived typical forecast error scenarios.

Step 4: Add each typical forecast error scenario to the base forecast power of RES and load to obtain their typical scenarios, which are used in the objective and constraints of the proposed Flexible low-carbon optimal dispatch model.

4.2 Objective function

The objective function of the proposed dispatch model is to minimize the total operation cost of the distribution network.

(1) The start-up and shut-down cost of the FCCGT

$$C^{\text{FCC}} = \sum_{t=1}^{T} \sum_{i=1}^{N_{\text{FCC}}} \left[c_i^{\text{u}} I_{i,t} \left(1 - I_{i,t-1}\right) + c_i^{\text{d}} I_{i,t-1} \left(1 - I_{i,t}\right) \right] \tag{15}$$

where i is the index of FCCGT. N_{FCC} is the total number of FCCGTs. c_i^{u} and c_i^{d} are the start-up and shut-down costs of the i-th FCCGT. $I_{i,t}$ and $I_{i,t-1}$ are the 0-1 variables indicating the states of the i-th FCCGT at time t and time $t-1$, respectively.

(2) The operational cost of the FCCGT

$$C^{\mathrm{R}} = \sum_{k=1}^{N_{\mathrm{sce}}} \sum_{t=1}^{T} \sum_{i=1}^{N_{\mathrm{FCC}}} p_k \left(c_{\mathrm{fuel}} P_{t,k,i}^{\mathrm{FCC}} + c_{\mathrm{ccus}} \chi M_{t,k,i}^{\mathrm{TC}} \right) \tag{16}$$

where k is the index of the typical scenarios. N_{sce} is the total number of typical scenarios. p_k is the weight coefficient of scenario k. c_{fuel} is the unit fuel cost of the FCCGT electricity generation. c_{ccus} is the unit operational cost of the CC device.

(3) The cost of purchasing power from the superior power grid

$$C^{\mathrm{Buy}} = \sum_{k=1}^{N_{\mathrm{sce}}} \sum_{t=1}^{T} p_k c_{\mathrm{grid},t} P_{\mathrm{e},t,k}^{\mathrm{buy}} \tag{17}$$

where $c_{\mathrm{grid},t}$ is the price of the power purchased from the superior power grid. $P_{\mathrm{e},t,k}^{\mathrm{buy}}$ is the quantity of purchased electricity.

(4) The subsidy cost for the DR incentive of MLEAF

$$C^{\mathrm{Mg}} = \sum_{k=1}^{N_{\mathrm{sce}}} \sum_{t=1}^{T} \sum_{m=1}^{N_{\mathrm{M}}} p_k \left(c_{\mathrm{m1}} P_{m,t,k}^{\mathrm{u}} + c_{\mathrm{m2}} P_{m,t,k}^{\mathrm{d}} \right) \tag{18}$$

where N_{M} is the total number of MLEAFs. c_{m1} and c_{m2} are the unit subsidies for increment and decrement responses of MLEAF, respectively.

(5) The carbon tax cost

This paper considers the implementation of a carbon tax policy in the distribution network and calculates the carbon tax cost associated with CO_2 emissions as follows:

$$C^{\mathrm{carb}} = c^{\mathrm{CO_2}} \sum_{k=1}^{N_{\mathrm{sce}}} \sum_{t=1}^{T} p_k \left(\sum_{i=1}^{N_{\mathrm{FCC}}} M_{t,k,i}^{\mathrm{GC}} + \lambda_e P_{\mathrm{e},t,k}^{\mathrm{buy}} \right) \tag{19}$$

where $c^{\mathrm{CO_2}}$ is the carbon tax price. λ_e is the average carbon emission factor corresponding to purchased electricity.

(6) The penalty cost for wind and solar power curtailment

$$C^{\mathrm{Curt}} = c^{\mathrm{cur}} \sum_{k=1}^{N_{\mathrm{sce}}} \sum_{t=1}^{T} p_k \left(\sum_{w=1}^{N_{\mathrm{w}}} \Delta P_{w,t,k}^{\mathrm{W}} + \sum_{v=1}^{N_{\mathrm{v}}} \Delta P_{v,t,k}^{\mathrm{PV}} \right) \tag{20}$$

where c^{cur} is the penalty price of curtailed wind and solar electricity. N_{w} and N_{v} are the number of wind farms and photovoltaic power stations, respectively. $\Delta P_{w,t,k}^{\mathrm{W}}$ and $\Delta P_{v,t,k}^{\mathrm{PV}}$ are the curtailed power of the w-th wind farm and the v-th photovoltaic power station, respectively.

(7) The load shedding cost

$$C^{\mathrm{LD}} = c^{\mathrm{L}} \sum_{k=1}^{n_{\mathrm{sce}}} \sum_{t=1}^{T} \sum_{b} p_k \Delta P_{b,t,k}^{\mathrm{L}} \tag{21}$$

where c^{L} is the penalty price of load shed. $\Delta P_{b,t,k}^{\mathrm{L}}$ is the load shed at bus b.

Based on (Equations 15–21), the total cost of the distribution network is calculated by Equation 22 as follows:

$$\min \quad C^{\mathrm{FCC}} + C^{\mathrm{R}} + C^{\mathrm{Buy}} + C^{\mathrm{Mg}} + C^{\mathrm{carb}} + C^{\mathrm{Curt}} + C^{\mathrm{LD}} \tag{22}$$

4.3 Constraints

(1) Constraints of FCCGT

The relevant constraints have been given by Equations 1–6.

(2) Constraints of MLEAF

The relevant constraints have been given by Equations 7–14.

(3) Power balance constraints

$$\begin{aligned} &P_{\mathrm{e},t,k}^{\mathrm{buy}} + \sum_{w} \left(P_{w,t,k}^{\mathrm{W}} - \Delta P_{w,t,k}^{\mathrm{W}} \right) + \sum_{v} \left(P_{v,t,k}^{\mathrm{PV}} - \Delta P_{v,t,k}^{\mathrm{PV}} \right) \\ &\quad = \sum_{b} \left(P_{b,t,k}^{\mathrm{Load}} - \Delta P_{b,t,k}^{\mathrm{L}} \right) + \sum_{m} P_{m,t,k} - \sum_{i=1}^{N_{\mathrm{FCC}}} P_{\mathrm{e},t,k,i}^{\mathrm{FCC}} \end{aligned} \tag{23}$$

where $P_{w,t,k}^{\mathrm{W}}$ and $P_{v,t,k}^{\mathrm{PV}}$ are the forecasted power of wind farm w and photovoltaic power station v. $P_{b,t,k}^{\mathrm{Load}}$ is the forecasted load power at bus b.

(4) Transmission capacity constraints of power lines

$$\begin{aligned} &\left| \sum_{b} K_{lb} \left[\sum_{b} P_{\mathrm{e},t,k}^{\mathrm{buy}} + \sum_{i \in b} P_{\mathrm{e},t,k,i}^{\mathrm{FCC}} + \sum_{w \in b} \left(P_{w,t,k}^{\mathrm{W}} - \Delta P_{w,t,k}^{\mathrm{W}} \right) + \right. \right. \\ &\left. \left. \sum_{v \in b} \left(P_{v,t,k}^{\mathrm{PV}} - \Delta P_{v,t,k}^{\mathrm{PV}} \right) - \left(P_{b,t,k}^{\mathrm{Load}} - \Delta P_{b,t,k}^{\mathrm{L}} \right) - \sum_{m \in b} P_{m,t,k} \right| \le f_{l\,\max} \end{aligned} \tag{24}$$

where K_{lb} is the power flow distribution factor of bus b to line l (Cai et al., 2022). $f_{l\max}$ is the maximum transmission power of line l.

(5) Wind and solar curtailment and load-shedding constraints

$$\begin{aligned} &0 \le \Delta P_{w,t,k}^{\mathrm{W}} \le P_{w,t,k}^{\mathrm{W}} \\ &0 \le \Delta P_{v,t,k}^{\mathrm{PV}} \le P_{v,t,k}^{\mathrm{PV}} \\ &0 \le \Delta P_{b,t,k}^{\mathrm{Load}} \le P_{b,t,k}^{\mathrm{L}} \end{aligned} \tag{25}$$

(6) Power output and ramp constraints of FCCGT

$$\begin{cases} I_{i,t} P_{\mathrm{e},i,\min}^{\mathrm{FCC}} \le P_{\mathrm{e},t,k,i}^{\mathrm{FCC}} \le I_{i,t} P_{\mathrm{e},i,\max}^{\mathrm{FCC}} \\ -DR_i \le P_{\mathrm{e},t,i}^{\mathrm{FCC}} - P_{\mathrm{e},t-1,i}^{\mathrm{FCC}} \le UR_i \end{cases} \tag{26}$$

where UR_i and DR_i are the maximum upward and downward ramp rate of the i-th FCCGT.

(7) Minimum duration constraints of on and off states of FCCGT

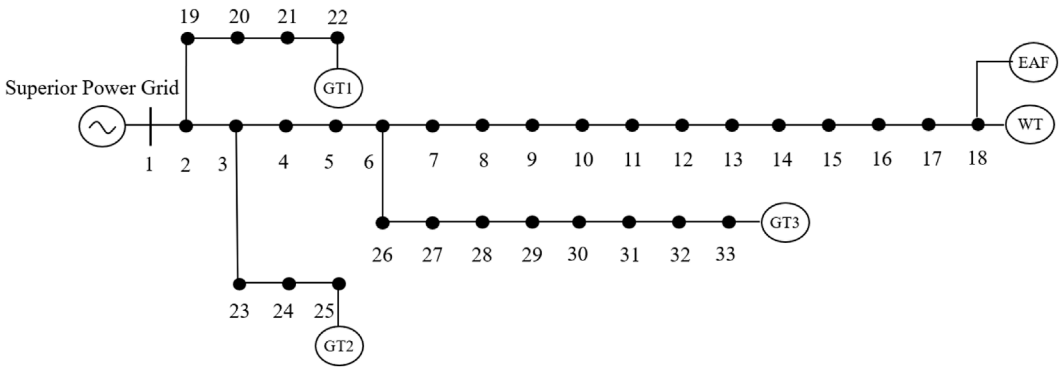

FIGURE 2
Test system based on a modified IEEE 33-bus standard system.

$$\begin{cases} \left(T_{i,t-1}^{\text{on}} - T_{i,\min}^{\text{on}}\right)\left(I_{i,t-1} - I_{i,t}\right) \geq 0 \\ \left(T_{i,t-1}^{\text{off}} - T_{i,\min}^{\text{off}}\right)\left(I_{i,t} - I_{i,t-1}\right) \geq 0 \end{cases} \tag{27}$$

where T_i^{on} and T_i^{off} are the minimum duration of on and off states of the i-th FCCGT. $I_{i,t}$ is a 0-1 variable which takes 1 for the on state and 0 for the off state. The constraints of the proposed flexible low-carbon dispatch model are finally composed of Equations 1–14 and Equations 23–27.

5 Numerical tests

5.1 Basic settings

A modified IEEE 33-bus standard system is designed as the test distribution system, whose network structure is shown in Figure 2. This designed system includes three identical FCCGTs, i.e., GT1-GT3, which are connected to buses 22, 25, and 33, respectively. The technical parameters of GT1-GT3 are shown in Table 1. The three FCCGTs have the same type of CC devices, with the parameters listed in Table 2.

The wind farm is connected to Bus 18, with its forecasted power output shown in Figure 3. The penalty price for curtailing wind power is 100 $/MW·h. Apart from MLEAF, the forecasted power of all the other loads in the distribution network is also shown in Figure 3. The ratio of load at each bus to the total load is the same with that in the original IEEE 33-bus standard system, which can be found in (Yang et al., 2021) and not elaborated here.

The MLEAF is connected to Bus 18. When not participating in DR project, the MLEAF daily power curve is a horizontal line with its value equal to the rated power. The relevant parameters are shown in Table 3.

The electricity price for purchasing power from the superior power grid adopts time-of-use pricing, where the peak, flat and valley periods are divided according to the load curve shape shown in Figure 3. The corresponding prices for each period are shown in Table 4. The average carbon emission factor for purchased electricity is 0.65 t/MW h.

TABLE 1 Parameters of FCCGT.

Parameter	Value
$P_{\max}^{\text{FCC}}$/MW	5
$P_{\min}^{\text{FCC}}$/MW	1.5
T^{on}/h	4
T^{off}/h	4
DR,UR/MW·h^{-1}	2
γ^{FCCGT}/t·(MW·h)$^{-1}$	0.24
SU, SD/$	32
c_{FCCGT}/$·(MW·h)$^{-1}$	14.35
c^{CO_2}/$·t^{-1}	20

TABLE 2 Parameters of CC device.

Parameter	Value
χ/MW·h·t^{-1}	0.27
$\theta_{\max}^{\text{CC}}$	1
η	1.2
M^{MEA}/g·mol^{-1}	61.08
M^{CO_2}/g·mol^{-1}	44
ψ	0.24
S^{MEA}	0.3
ρ^{MEA}/g·ml^{-1}	1.01
V^{L}/m^3	1,500

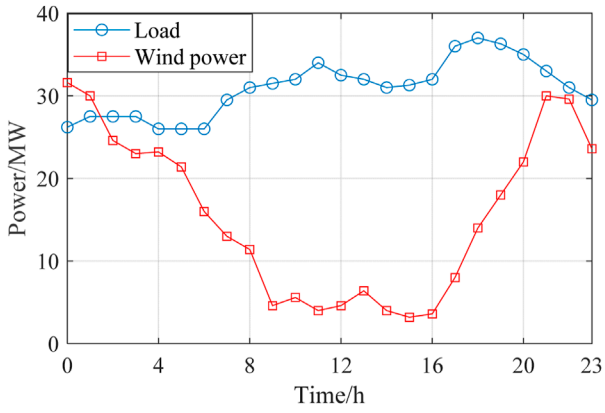

FIGURE 3
The forecasted power of the wind farm and load.

TABLE 3 Parameters of MLEAF.

Parameter	Value
P_m^{base}/MW	5
$P_m^{\text{r,d}}$, $P_m^{\text{r,u}}$/MW	4.7, 5.5
$P_{m,t}^{\text{u}}$, $P_{m,t}^{\text{d}}$/MW	1.75, 1.05
c_{m1}, c_{m2}/\$·(MW·h)$^{-1}$	5.02, 3.58
M	7
O/t	52
λ_1/t·(MW·h)$^{-1}$	0.286
λ_2/t·(MW·h)$^{-1}$	0.333
λ_3/t·(MW·h)$^{-1}$	0.357

Based on the parameters above, three different scenarios are designed for comparative analysis to verify that the incorporation of FCCGT and DR of MLEAF can improve the economic efficiency, low-carbon attribute and flexibility of the distribution network. These scenarios are as follows.

Scenario 1: GT1-GT3 are equipped with CC devices without solution storage tanks and with a fixed flue gas diversion ratio. The MLEAF does not participate in the DR project.

Scenario 2: GT1-GT3 are FCCGTs with adjustable flue gas diversion ratios. The MLEAF does not participate in the DR project.

Scenario 3: GT1-GT3 are FCCGTs with adjustable flue gas diversion ratios. The MLEAF takes part in the DR project. This scenario corresponds to the flexible low-carbon optimal dispatch model proposed in Section 4.

All three scenarios are modeled with the YALMIP toolbox and solved by the CPLEX solver on the MATLAB platform.

5.2 Comparison and analysis of dispatch results for the three scenarios

The dispatch costs are shown in Table 5.

According to Table 5, it can be found that.

1) In Scenario 2, the carbon emission is reduced by 18 t compared to Scenario 1. The wind power curtailment penalty is decreased by 4,340 \$. The total cost is decreased by 8,000 \$. This indicates that the FCCGT has higher flexibility than gas turbines equipped with CC devices without solution storage tanks, which improves CC efficiency and promotes the utilization of renewable energy.
2) In Scenario 3, carbon emission is reduced by 14 t compared to Scenario 2. The total cost is decreased by 9.7×10^4 \$ and 1.7×10^4 \$ compared to Scenario 1 and Scenario 2, respectively. This indicates that, incorporating the DR of MLEAF into the distribution network dispatch can significantly improve the energy utilization efficiency, effectively reduce the peak loads and lower the carbon emission.

In summary, the effectiveness of the proposed flexible low-carbon optimal dispatch model is validated by comparing the total costs, carbon emissions and wind curtailment of the three scenarios.

The dispatch schemes of the three scenarios are shown in Figures 4–6.

According to Figures 4–7, the outputs of all the power sources during the peak load periods are compared between the three scenarios. It can be found that the proposed model can optimize the output of FCCGTs and the wind farm, so the distribution network can effectively interact with the superior power grid to achieve the "peak shaving and valley filling" effect. More specifically, during peak periods, the external power purchase is decreased by utilizing MLEAF to reduce its own load. During off-peak periods, the consumption of wind power is increased through reasonable dispatching, which also reduces the external power purchase. Since the carbon emission factor of purchased electricity is higher than that of gas turbines and wind power, the proposed model results in a decrease in the total daily carbon emissions, which proves its low-carbon property.

According to Figures 8, 9, the fixed gas diversion ratio in Scenario 1 results in a nearly constant high CC power during peak periods, which further leads to a shortage in the feed-in power of the FCCGTs and exacerbates the power generation deficit. In Scenarios 2 and 3, CO_2 that cannot be processed during peak periods is stored in the solution tanks and processed later in the off-peak periods. In this way, the CC power consumption during peak periods is reduced to zero, which allows FCCGTs to provide more feed-in power during peak periods and more CO_2 processing load during off-peak periods. Such flexibility promotes RES power consumption and achieves peak-shaving and valley-filling effects.

According to Figure 10, during the peak period from 18:00 to 20:00, the gas diversion ratio in Scenario 3 is higher than that in Scenario 2. This is because the DR of the MLEAF alleviates the power output pressure of FCCGTs during peak periods. More specifically, MLEAF actively responds to the distribution network's peak shaving instructions and reduces its load demand, so the required power output and the corresponding CO_2 generated by FCCGTs are both lowered. Therefore, FCCGTs can provide more CC power to process

TABLE 4 Time period division and electricity price.

Time	0:00–6:00	7:00–10:00 13:00–16:00 22:00–23:00	11:00–12:00 17:00–21:00
Load situation	Valley	Flat	Peak
Price/$·(MW·h)$^{-1}$	43.04	86.08	172.16

TABLE 5 Comparison of distribution network operating costs under different scenarios.

Indicator	Scenario 1	Scenario 2	Scenario 3
Gas turbine operating cost/$	3.58×10^3	3.56×10^3	3.50×10^3
Purchased electricity cost/$	3.08×10^5	2.33×10^5	2.17×10^5
Carbon tax cost/$	3.87×10^3	3.51×10^3	3.23×10^3
Wind curtailment cost/$	8.39×10^3	4.05×10^3	3.20×10^3
EAF load adjustment cost/$	—	—	1.06×10^2
Total cost/$	3.24×10^5	2.44×10^5	2.27×10^5
Carbon emission/t	1.93×10^2	1.75×10^2	1.61×10^2

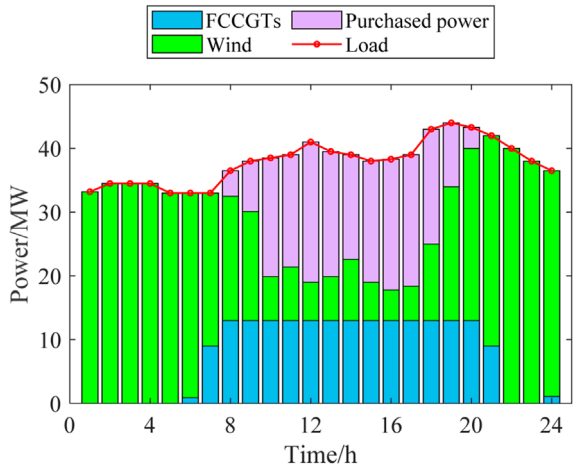

FIGURE 5
Dispatch scheme of scenario 2.

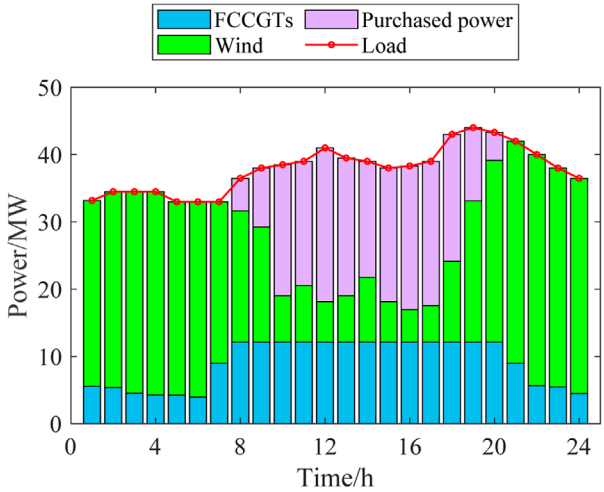

FIGURE 4
Dispatch scheme of scenario 1.

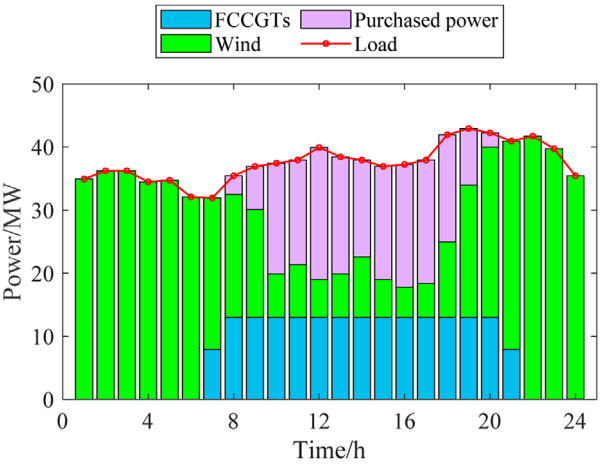

FIGURE 6
Dispatch scheme of scenario 3.

the smaller amount of carbon emission, which results in the higher flue gas diversion ratio in Scenario 3.

According to Figure 11, the solution volumes in the rich and lean solution tanks vary with time to react with the operation condition of the distribution network. During the peak periods, the MEA solution volume in the rich solution tank increases, which indicates that CC power is reduced in these periods and CO_2 is stored temporarily for later processing. During the valley periods, MEA flows out of the rich solution tank to release CO_2 and then flows into the lean solution tank, which indicates that the CC power increases to process the CO_2 temporarily stored in peak periods.

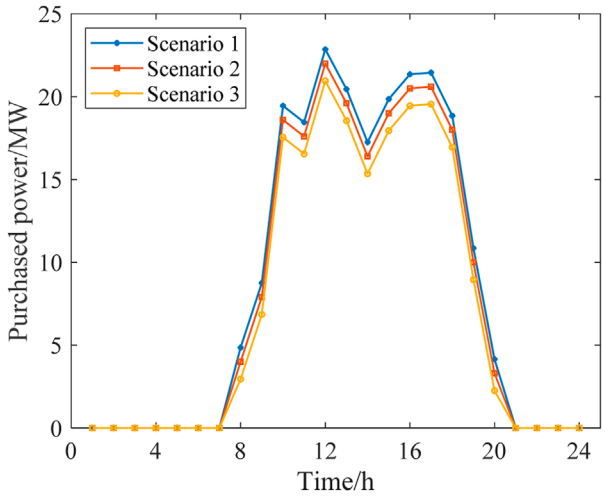

FIGURE 7
Power purchased from the superior power grid of 3 scenarios.

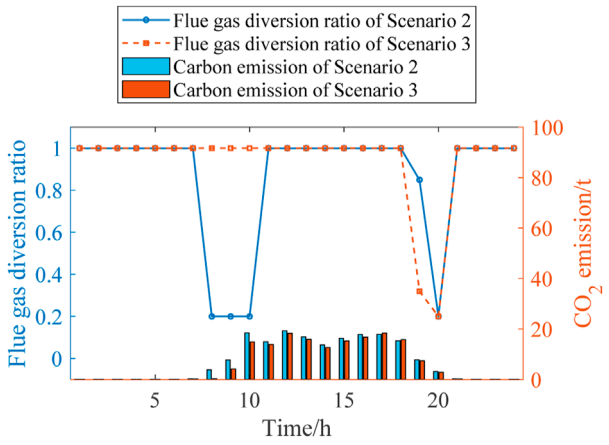

FIGURE 10
Flue gas diversion ratios and captured carbon of scenario 2 and scenario 3.

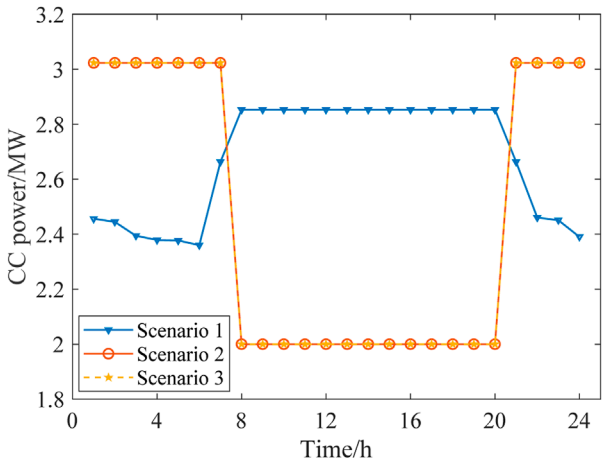

FIGURE 8
Power consumed by CC devices of 3 scenarios.

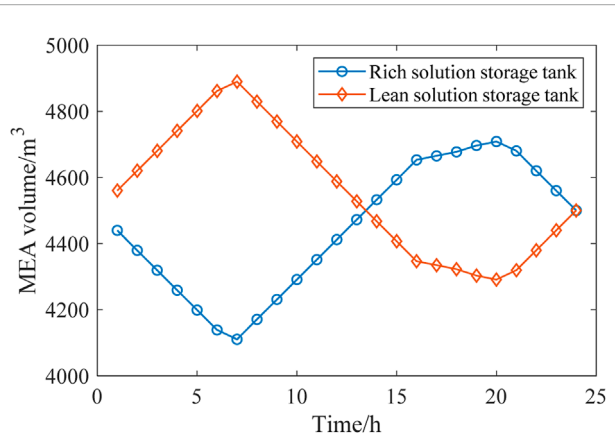

FIGURE 11
Stored MEA solution in the rich and lean solution tanks of scenario 2.

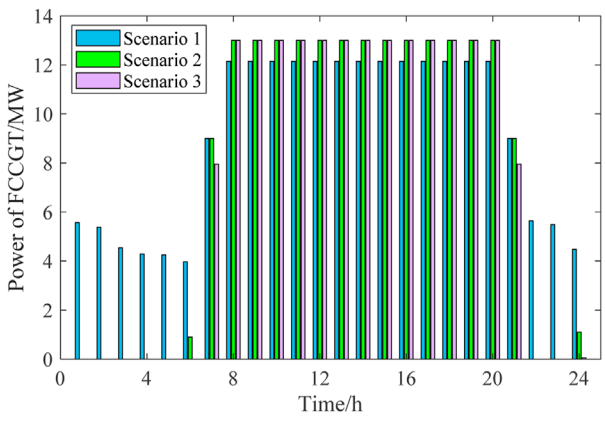

FIGURE 9
Feed-in power of FCCGTs of 3 scenarios.

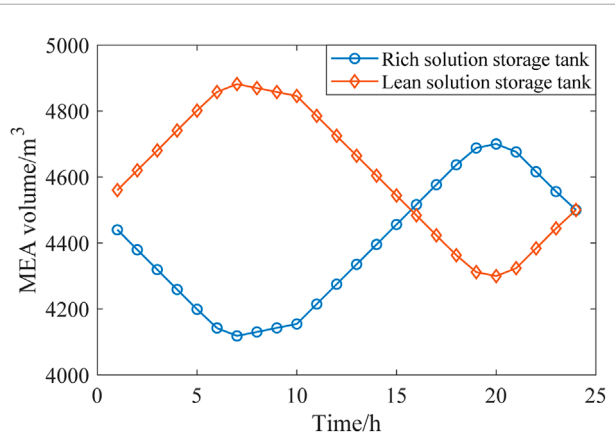

FIGURE 12
Stored MEA solution in the rich and lean solution tanks of scenario 3.

Through the coordinated operation of the rich and lean solution tanks, the CC amount and the CC power consumption are decoupled, contributing to the flexible low-carbon economic dispatch of the distribution network.

From the comparison of Figures 11, 12, it can be observed that compared to Scenario 2, Scenario 3 additionally considers the flexibility brought by the DR of MLEAF. Therefore, the CC devices can operate more efficiently across different load periods, which better balances the operating efficiency and energy consumption of the FCCGTs. With the flexibility from both the generation and load sides, the overall efficiency and stability of the distribution network is improved, which means lower operation costs and smaller environmental impact.

6 Conclusion

A novel flexible low-carbon optimal dispatch model is proposed in this paper for the distribution network, which coordinates FCCGTs and the DR of MLEAF to achieve balances between the operation efficiency, carbon emissions, RES power curtailment and load shedding amount. The correctness and advantages of the proposed model is verified by designed numerical tests. The specific conclusions are as follows:

1) By modelling the flexibility provided by the solution tanks and flue gas diversion system of FCCGTs, the carbon emission and processing is effectively controlled by the CC devices, which improves the utilization efficiency of fossil energy in the optimal dispatch of the distribution network.
2) The cooperation of the FCCGTs and the DR of MLEAF avoids the frequent start and stop of FCCGTs and alleviates the pressure peak regulation. Under this condition, the distribution network can operate in more stable and efficient mode, which realizes the environmental sustainability and economic benefits.

Data availability statement

The original contributions presented in the study are included in the article/supplementary material, further inquiries can be directed to the corresponding author.

Author contributions

WW: Funding acquisition, Methodology, Software, Supervision, Writing–original draft, Writing–review and editing. HH: Conceptualization, Data curation, Software, Supervision, Writing–review and editing. XZ: Data curation, Project administration, Resources, Validation, Writing–review and editing. JT: Conceptualization, Formal Analysis, Validation, Writing–review and editing. SS: Conceptualization, Supervision, Validation, Writing–review and editing.

Funding

The author(s) declare that financial support was received for the research, authorship, and/or publication of this article. The financial aid received from Jiangsu Provincially Managed Industrial Projects (JC2024003) is gratefully acknowledged.

Conflict of interest

Authors WW, HH, and SS were employed by Nanjing Suyi Industrial Co., Ltd. Author XZ was employed by Nanjing Suyi Industrial Co., Ltd. Author JT was employed by Nanjing Huaqun Energy Group Co., Ltd.

Generative AI statement

The author(s) declare that no Generative AI was used in the creation of this manuscript.

Publisher's note

All claims expressed in this article are solely those of the authors and do not necessarily represent those of their affiliated organizations, or those of the publisher, the editors and the reviewers. Any product that may be evaluated in this article, or claim that may be made by its manufacturer, is not guaranteed or endorsed by the publisher.

References

Boldrini, A., Koolen, D., Crijns-Graus, W., Worrell, E., and van den Broek, M. (2024). Flexibility options in a decarbonising iron and steel industry. *Renew. Sustain. Energy Rev.* 189, 113988. doi:10.1016/j.rser.2023.113988

Cai, J., Hao, L., Xu, Q., and Zhang, K. (2022). Reliability assessment of renewable energy integrated power systems with an extendable Latin hypercube importance sampling method. *Sustain Energy Techn* 50, 101792. doi:10.1016/j.seta.2021.101792

Cheng, L., Zang, H., Wei, Z., and Sun, G. (2023). Secure multi-party household load scheduling framework for real-time demand-side management. *IEEE T Sustain Energ* 14 (1), 602–612. doi:10.1109/tste.2022.3221081

Chyong, C. K., Reiner, D. M., Ly, R., and Fajardy, M. (2023). Economic modelling of flexible carbon capture and storage in a decarbonised electricity system. *Renew. Sust. Energ Rev.* 188, 113864. doi:10.1016/j.rser.2023.113864

Condessa, G. Á., Ismail, K. A. R., Hunt, J. D., Ponce Júnior, N., Velásquez, R. M. G., Borges, V. L., et al. (2023). Electricity generation potential from natural gas pressure reduction turbines in Brazil. *Energ Effic.* 16 (8), 97. doi:10.1007/s12053-023-10176-8

de Chalendar, J. A., McMahon, C., Fuentes Valenzuela, L., Glynn, P. W., and Benson, S. M. (2023). Unlocking demand response in commercial buildings: empirical response of commercial buildings to daily cooling set point adjustments. *Energ Build.* 278, 112599. doi:10.1016/j.enbuild.2022.112599

Deng, L., Sun, H., Li, B., Sun, Y., Yang, T., and Zhang, X. (2021). Optimal operation of integrated heat and electricity systems: a tightening McCormick approach. *Engineering* 7 (8), 1076–1086. doi:10.1016/j.eng.2021.06.006

Fan, W., Ju, L., Tan, Z., Li, X., Zhang, A., Li, X., et al. (2023). Two-stage distributionally robust optimization model of integrated energy system group considering energy sharing and carbon transfer. *Appl. Energ* 331, 120426. doi:10.1016/j.apenergy.2022.120426

Gabrielli, P., Campos, J., Becattini, V., Mazzotti, M., and Sansavini, G. (2022). Optimization and assessment of carbon capture, transport and storage supply chains for industrial sectors: the cost of resilience. *Int. J. Greenh. Gas. Con* 121, 103797. doi:10.1016/j.ijggc.2022.103797

Gao, X., Wang, S., Sun, Y., and Zhai, J. (2024). Low-carbon operation of integrated electricity-gas system with hydrogen injection considering hydrogen mixed gas turbine and laddered carbon trading. *Appl. Energ* 374, 123902. doi:10.1016/j.apenergy.2024.123902

Huang, Y., Chen, S., Chen, Z., Hu, W., and Huang, Q. (2020). Improved probabilistic load flow method based on D-vine copulas and Latin hypercube sampling in distribution network with multiple wind generators. *IET Generation, Transm. and Distribution* 14 (5), 893–899. doi:10.1049/iet-gtd.2019.1126

Qi, X., Zhao, T., Liu, X., and Wang, P. (2023). Three-Stage stochastic unit commitment for microgrids toward frequency security via renewable energy deloading. *IEEE T Smart Grid* 14 (6), 4256–4267. doi:10.1109/tsg.2023.3263273

Shao, C., Feng, C., Shahidehpour, M., Zhou, Q., Wang, X., and Wang, X. (2021). Optimal stochastic operation of integrated electric power and renewable energy with vehicle-based hydrogen energy system. *IEEE T Power Syst.* 36 (5), 4310–4321. doi:10.1109/tpwrs.2021.3058561

Song, J., Zhang, Z., Mu, Y., Wang, X., Chen, H., Pan, Q., et al. (2024). Enhancing environmental sustainability via interval optimization for low-carbon economic dispatch in renewable energy power systems: leveraging the flexible cooperation of wind energy and carbon capture power plants. *J. Clean. Prod.*, 442. doi:10.1016/j.jclepro.2024.140937

Tan, W. S., Shaaban, M., and Ab Kadir, M. Z. A. (2019). Stochastic generation scheduling with variable renewable generation: methods, applications, and future trends. *IET Generation, Transm. and Distribution* 13 (9), 1467–1480. doi:10.1049/iet-gtd.2018.6331

Wang, J., Wang, Q., and Sun, W. (2023a). Quantifying flexibility provisions of the ladle furnace refining process as cuttable loads in the iron and steel industry. *Appl. Energ* 342, 121178. doi:10.1016/j.apenergy.2023.121178

Wang, W., Chai, T., Wang, H., and Wu, Z. (2023b). Signal-compensation-based adaptive PID control for fused magnesia smelting processes. *IEEE T Ind. Electron* 70 (9), 9441–9451. doi:10.1109/TIE.2022.3212392

Wang, Y., Gao, S., Jia, W., Ding, T., Zhou, Z., and Wang, Z. (2022). Data-driven distributionally robust economic dispatch for park integrated energy systems with coordination of carbon capture and storage devices and combined heat and power plants. *IET Renew. Power Gen.* 16 (12), 2617–2629. doi:10.1049/rpg2.12436

Wang, Y., Yang, Z., Zhao, X., Liu, H., Wang, D., and Liu, C. (2024). Fine-grained modeling and coordinated scheduling of source-load with energy-intensive electro-fused magnesium loads. *IEEE Access* 12, 47702–47712. doi:10.1109/access.2024.3381781

Wilkes, M. D., Mukherjee, S., and Brown, S. (2021). Transient CO 2 capture for open-cycle gas turbines in future energy systems. *Energy* 216, 119258. doi:10.1016/j.energy.2020.119258

Xu, D., Xiang, S., Bai, Z., Wei, J., and Gao, M. (2023). Optimal multi-energy portfolio towards zero carbon data center buildings in the presence of proactive demand response programs. *Appl. Energ* 350, 121806. doi:10.1016/j.apenergy.2023.121806

Xu, J., and Yi, Y. (2023). Multi-microgrid low-carbon economy operation strategy considering both source and load uncertainty: a Nash bargaining approach. *Energy (Oxford)* 263, 125712. doi:10.1016/j.energy.2022.125712

Yang, M., Li, J., Li, J., Yuan, X., and Xu, J. (2021). Reconfiguration strategy for DC distribution network fault recovery based on hybrid particle swarm optimization. *Energies* 14 (21), 7145. doi:10.3390/en14217145

Yue, X., Liao, S., Xu, J., Ke, D., Wang, H., Yang, J., et al. (2024). Collaborative optimization of renewable energy power systems integrating electrolytic aluminum load regulation and thermal power deep peak shaving. *Appl. Energ* 373, 123869. doi:10.1016/j.apenergy.2024.123869

Zhang, B., Hu, W., Ghias A, M. Y. M., Xu, X., and Chen, Z. (2023). Multi-agent deep reinforcement learning based distributed control architecture for interconnected multi-energy microgrid energy management and optimization. *Energ Convers. Manage* 277, 116647. doi:10.1016/j.enconman.2022.116647

Zhang, S., Qiu, G., Liu, Y., Ding, L., and Shui, Y. (2024). Data-Driven distributionally robust optimization-based coordinated dispatching for cascaded hydro-PV-PSH combined system. *Electronics-Switz.* 13 (3), 667. doi:10.3390/electronics13030667

Zhang, W., and Zhu, T. (2024). Flexible resource demand response scheduling strategy under 5G-V2X. *Sustain. Energy, Grids Netw.* 39, 101441. doi:10.1016/j.segan.2024.101441

Zhang, Y., Liu, Y., Shu, S., Zheng, F., and Huang, Z. (2021). A data-driven distributionally robust optimization model for multi-energy coupled system considering the temporal-spatial correlation and distribution uncertainty of renewable energy sources. *Energy* 216, 119171. doi:10.1016/j.energy.2020.119171

Zhao, X., Wang, Y., Liu, C., Cai, G., Ge, W., Zhou, J., et al. (2024). Low carbon scheduling method of electric power system considering energy-intensive load regulation of electrofused magnesium and wind power fluctuation stabilization. *Appl. Energ* 357, 122573. doi:10.1016/j.apenergy.2023.122573

Nomenclature

Abbreviations

RES	renewable energy sources
CC	carbon capture
FCCGT	gas turbines installed with flexible CC technology
HSIL	heat storage industrial loads
DR	demand response
MLEAF	magnesium load using an electric arc furnace

Indices

t	index of time
i	index of FCCGT
w	index of wind farms
v	index of photovoltaic power stations
b	index of load buses
l	index of line
m	index of MLEAF

Variables

P_t^{FCC}	total power output of FCCGT
$P_{\mathrm{e},t}^{\mathrm{FCC}}$	FCCGT power delivered to distribution network
P_t^{Y}	power consumption of the CC device
M_t^{TC}	total mass of the captured CO_2
M_t^{UC}	mass of CO_2 supplied from/absorbed by the rich solution storage tank
δ_t	flue gas diversion ratio
M_t^{AC}	total mass of CO_2 produced by FCCGT
M_t^{GC}	mass of CO_2 emitted to the atmosphere by FCCGT
V_t^{in}, V_t^{out}	MEA volume flowing into/out of the rich solution storage tank
S_t^{MEA}	solution concentration
ρ_t^{MEA}	solution density
$V_t^{\mathrm{F}} V_t^{\mathrm{W}}$	MEA volumes in rich/lean solution storage tanks U_t^{F}, U_t^{W} 0-1 variables indicating the MEA volume changes in the rich/lean solution storage tanks
$P_{m,t}$	operating power of the MLEAF after regulation
$P_{m,t}^{\mathrm{u}}$	power increment of the MLEAF
$\lambda_{m,t}$	yield rate of the m-th MLEAF at time t
$I_{i,t}$	0-1 variables indicating the states of FCCGT i
$c_{\mathrm{grid},t}$	price of power purchased from superior power grid
$P_{\mathrm{e},t,k}^{\mathrm{buy}}$	quantity of purchased electricity
$\Delta P_{w,t,k}^{\mathrm{W}}$	curtailed power of wind farm w
$\Delta P_{v,t,k}^{\mathrm{PV}}$	curtailed power of the photovoltaic station v
$\Delta P_{b,t,k}^{\mathrm{L}}$	load shed at bus b
$P_{w,t,k}^{\mathrm{W}}$	forecasted power of wind farm w
$P_{v,t,k}^{\mathrm{PV}}$	forecasted power of photovoltaic station v
$P_{b,t,k}^{\mathrm{Load}}$	forecasted load power at bus b

Parameters

χ	consumed power for capturing unit mass of CO_2
$\theta_{\mathrm{max}}^{\mathrm{CC}}$	maximum CC level
γ^{FCC}	CO2 emission intensity of FCCGT
$P_{\mathrm{max}}^{\mathrm{FCC}}$, $P_{\mathrm{min}}^{\mathrm{FCC}}$	upper and lower power limits of FCCGT
M^{MEA}	molar masses of MEA
$M^{\mathrm{CO_2}}$	molar masses of CO_2
ψ	mass of CO_2 that can be absorbed by 1 mol of MEA
T	total time slots in a dispatching cycle
V^{L}	volume of the solution storage tanks
P_m^{base}	rated power of MLEAF m
$P_{\mathrm{max}}^{\mathrm{u}}$, $P_{\mathrm{max}}^{\mathrm{d}}$	maximum power increment/decrement of MLEAF
O_m	target of MLEAF production output
$\lambda_1, \lambda_2, \lambda_3$	the MLEAF yield rates under the power decrease/nominal/increase state
N_{FCC}	total number of FCCGTs
c_i^{u}, c_i^{d}	start-up/shut-down costs of FCCGT i
N_{sce}	total number of scenarios
p_k	weight coefficient of scenario k
c_{fuel}	unit fuel cost of the FCCGT electricity generation
c_{ccus}	unit operational cost of the CC device
N_{M}	total number of MLEAFs
c_{m1}, c_{m2}	unit subsidy of increment/decrement response of MLEAF
$c^{\mathrm{CO_2}}$	carbon tax price
λ_e	carbon emission factor of purchased electricity
c^{cur}	penalty price of curtailed wind and solar electricity
N_{w}	the number of wind farms
N_{v}	the number of photovoltaic power stations
c^{L}	penalty price of load shed
UR_i,DR_i	upward/downward ramp rate of FCCGT i
T_i^{on}, T_i^{off}	minimum duration of on/off states of FCCGT i